Endorsed by **IPEM** Institute of Physics and Engineering in Medicine

PURPOSE-LED PUBLISHING™

PAPER • OPEN ACCESS

A Monte Carlo dose engine for fast neutron therapy and boron neutron capture therapy for matRad

View the article online for updates and enhancements.

Biomedical Physics & Engineering Express

PAPER

A Monte Carlo dose engine for fast neutron therapy and boron neutron capture therapy for matRad

Lucas Sommer[1,2,3,*] ⓘ, **Tobias Chemnitz**[2] ⓘ, **Niklas Wahl**[4,5] ⓘ, **Amit B A Bennan**[4,5] ⓘ,
Stephanie E Combs[3,6] ⓘ and **Jan J Wilkens**[1,3] ⓘ

1 Technical University of Munich (TUM), TUM School of Natural Sciences, Physics Department, Garching, Germany
2 TUM, Heinz Maier-Leibnitz Zentrum (MLZ), Garching, Germany
3 TUM, TUM School of Medicine and Health and Klinikum rechts der Isar, Department of Radiation Oncology, Munich, Germany
4 Department of Medical Physics in Radiation Oncology, German Cancer Research Center (DKFZ), Heidelberg, Germany
5 National Center for Radiation Oncology (NCRO), Heidelberg Institute for Radiation Oncology (HIRO), Heidelberg, Germany
6 Institute of Radiation Medicine (IRM), Helmholtz Zentrum München GmbH, German Research Center for Environmental Health,
   Neuherberg, Germany
* Author to whom any correspondence should be addressed.

E-mail: lucas.sommer@tum.de

Abstract

Objective: The purpose of the work presented here was to enable easy access to Monte Carlo dose calculation for both fast neutron therapy and boron neutron capture therapy for research purposes. The dose calculation approach was especially intended to hold high customization potential for individual user applications. *Approach:* The dose engine is based on the Monte Carlo code MCNP. It is integrated into the MATLAB-based open source research treatment planning software matRad as modular component. *Main results:* Total dose calculation is enabled for both fast neutron therapy and boron neutron capture therapy on patient CT data. The evaluation of the dose distribution is possible using the matRad graphical user interface and dose volume histograms. Customization options are provided for advanced users. *Significance:* The open source treatment planning software allows easy access to highly accurate Monte Carlo dose calculation for research projects.

1. Introduction

The use of neutrons in radiation therapy was first considered by Locher (1936) who discussed the therapeutic possibilities of both fast and slow neutrons. As already considered by Locher, basically two treatment modalities - fast neutron therapy (FNT) and neutron capture therapy - have been investigated over the last nine decades with varying stages of availability and clinical acceptance. Neutrons are classified depending on their energy as thermal with $E_n \leqslant 0.5$ eV, epithermal with 0.5 eV $< E_n \leqslant 10$ keV, and fast with $E_n > 10$ keV (IAEA 2023). Different properties of the incident neutrons are exploited for the two treatment modalities. Fast neutrons have high enough energy to produce recoil protons or heavier secondary ions that in turn produce ionizations along their tracks leading to cell damage. Neutron capture therapy is mainly performed with boron and then

called boron neutron capture therapy (BNCT). The boron isotope B-10 is supposed to be brought into tumor cells so that the high cross section for thermal neutron capture reactions of B-10 can be exploited for cell selective radiotherapy with neutrons. Upon neutron irradiation, B-10 disintegrates into an alpha particle (He-4) and a recoil lithium nucleus (Li-7) leading to localized dose deposition. Due to the produced secondary charged particles, both modalities provide high linear energy transfer (LET) treatments (cf Jones (2020) & Suzuki (2020)).

The experience collected with FNT over the last decades is summarized in several general and facility-specific review articles, for example by Jones and Wambersie (2007), Specht *et al* (2015), Jones (2020), and Gordon *et al* (2022). All mentioned publications indicate a high biological effectiveness and a low enhancement by cell oxygenation for fast neutrons as well as a low dependency of the biological effect on the

cell cycle. While enthusiastically followed in the 1970s through 1980s, FNT was abandoned by many centers due to the observed greater normal tissue toxicity in comparison to low LET radiation (Specht *et al* (2015) & Moffitt *et al* (2020)).

For some specific treatment indications, remaining interest in the clinical application of FNT as high-LET radiation modality is present. This is reflected in recent retrospective publications as for example performed by Loap and Kirova on breast cancer (Loap and Kirova 2021) or Aljabab *et al* (Aljabab *et al* 2021) on recent experience with irradiation of salivary gland tumors in a combined neutron-proton treatment approach.

To our best knowledge, today only one FNT facility is actively treating cancer patients. At the clinical neutron therapy system (CNTS) of the University of Washington in Seattle, USA, high-energy fast neutrons are generated from protons with $E = 50.5$ MeV incident on a beryllium target (Moffitt *et al* 2018). The neutrons produced by the CNTS have depth-dose characteristics similar to 6 MV x-rays (Moffitt *et al* 2018) which offers additional skin sparing in contrast to lower neutron energies. The delivery of intensity modulated neutron therapy (IMNT) was introduced with the CNTS in October 2022 ((Sandison *et al* 2023) & (Anderson *et al* 2023)). In addition, a newly developed imaging device for patient-specific IMNT quality assurance was recently introduced (Lehnert *et al* 2025). Patient treatment in the last remaining FNT facilities in Russia was recently stopped (Gulidov *et al* 2023).

In contrast to FNT, BNCT is currently experiencing a renaissance especially in China and Japan (Barth *et al* 2024). In Japan, BNCT was listed in 2020 as a treatment option reimbursed by Japanese health insurance companies. One of the driving factors of the renaissance BNCT is currently experiencing is the recent development of compact accelerator based neutron sources that can be installed directly in hospitals (Sauerwein *et al* 2023). This greatly improves the accessibility of neutrons and therefore the feasibility of BNCT.

For both modalities of neutron therapy, accurate state of the art dose calculation is necessary. As highlighted by Jones (2020) for FNT, not including variations of proton recoils from neutron interaction with the hydrogen content in an accurate way in routine dose calculation was one of the reasons why FNT failed to fulfill its original promises. For BNCT, accurate modeling of high LET interactions in treatment planning will be of similar importance as for FNT. This modeling of high LET radiation will include tissue and radiation-type dependencies as well as the dose-dependence of the relative biological effectiveness (RBE) with reference to Co-60 radiation. In order to do so, different models like the local effect model, the microdosimetric-kinetic model and the repair-

misrepair-fixation model were developed and are reviewed by Stewart *et al* (2018).

In general, the commercial availability of treatment planning systems (TPS) for BNCT will be a key factor for the wide acceptance of BNCT (Barth *et al* 2024). While for a long period of time only customized solutions were available for both FNT and BNCT (Kalet *et al* (2013) & Barth *et al* (2024)), a commercial interest in TPS for BNCT is awakened (Ray-Search (2024) & Neuboron (2024)). Also, a highly advanced customized solution was realized in the recent past for FNT with the CNTS in Seattle (Moffitt *et al* (2020), Sandison *et al* (2023), & Moffitt *et al* (2023)).

At the research neutron source FRM II in Garching, the medical applications facility MEDAPP provides fast fission neutrons for FNT (Wagner *et al* 2008). An extended area source for fission of uranium U-235 is used to provide neutrons. While no patients were treated at MEDAPP since 2015, it is currently undergoing a general upgrade program in order to re-establish FNT in Garching. Since no commercial solution is available, the work presented here started off with the goal to provide a dose calculation software for MEDAPP for retrospective dose calculations and research purposes.

For this purpose, a Monte Carlo dose engine based on MCNP was integrated into the open source research treatment planning software matRad (Wieser *et al* (2017) & Abbani *et al* (2024)). The presented matRad extension for neutrons as part of the open source treatment planning infrastructure allows easy access and provides high flexibility for customization for research projects addressing FNT or BNCT. For example, the evaluation of different neutron spectra or beam shaping assembly solutions can be realized in combination with highly accurate Monte Carlo simulation studies on patient CT data. Furthermore, the dose engine can help to facilitate multi-modality simulation studies including neutron therapy as performed for example partly using matRad for carbon ion therapy in combination with BNCT by Han *et al* (2023).

2. Methods

2.1. Monte Carlo integration in matRad

The presented dose calculation engine is based on the general-purpose Monte Carlo (MC) code MCNP 6.2 which allows transport calculations for neutron and gamma radiation as well as for all secondary charged particles relevant for radiotherapy (Werner 2017). The dose engine was integrated as a modular component to run within the MATLAB-based open source research treatment planning software matRad (Wieser *et al* (2017) & Abbani *et al* (2024)). Here, neutrons were added as an
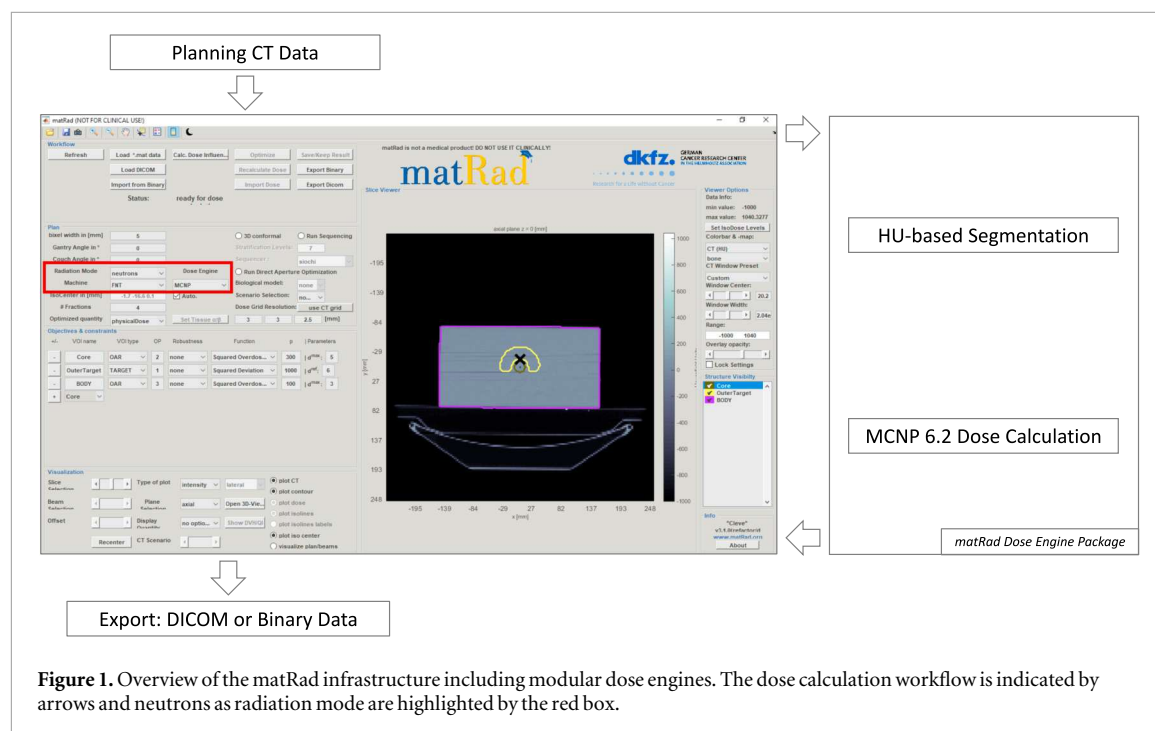
Figure 1. Overview of the matRad infrastructure including modular dose engines. The dose calculation workflow is indicated by arrows and neutrons as radiation mode are highlighted by the red box.

Table 1. Elemental tissue composition in weight-% used for MC simulations according to ICRU ICRU (1992) (soft tissue, lung, and skin), DeMarco *et al* (1998) (bone), and NIST (NIST 2022) (air).

	H	C	N	O	Na	P	S	Cl	Ar	K	Ca
Soft tissue	10.1	11.1	2.6	76.2	—	—	—	—	—	—	—
Lung	10.3	10.4	3.1	74.9	0.2	0.2	0.3	0.3	—	0.2	—
Skin	10.0	20.4	4.2	64.5	0.2	0.1	0.2	0.3	—	0.1	—
Bone	3.4	15.5	4.2	43.5	—	10.3	—	—	—	—	22.5
Air	—	—	75.5	23.2	—	—	—	—	1.3	—	—

independent radiation modality and integrated into the modular *DoseEngines* package within matRad as shown in figure 1. matRad provides all features necessary for forward and inverse treatment planning like an import tool for planning CT data given in DICOM standard, a dose-matrix-based optimization algorithm for intensity modulated radiation therapy (IMRT), and dose visualization and evaluation functions. The modifications were implemented to be compatible with the infrastructure of the *DoseEngine* package in matRad version *Cleve* v3.1.0 which was released in 2024 by the German Cancer Research Center (DKFZ). The implementation at the state of submission was based on matRad 3.1.0 (Abbani *et al* 2024) and is available on the branch *research/neutrons* of the main matRad repository [7]. The simulations discussed in the following were run in parallel mode on a virtual Windows 10 machine. The virtual machine runs on a cluster and is attributed with 48 Xeon Platinum 8160 CPUs with 2.1 GHz and two logical processors each and 130 GB of RAM.

Table 2. Hounsfield unit intervals for tissue segmentation of CT data.

Material	Air	Lung tissue	Soft tissue	Bone
HU values	< -950	-950 to -200	-200 to 280	> 280

2.2. Material definition and segmentation

For the Monte Carlo simulation of radiation transport and dose deposition in the patient, the relative elemental tissue compositions (in weight-%) are defined as given in table 1. *Soft tissue, lung tissue, and skin tissue* are defined as tabulated for adults in ICRU report 46 (ICRU 1992) and *cortical bone* is defined according to DeMarco *et al* (1998). For air, the elemental composition is defined according to the material tables provided by NIST NIST (2022).

On a voxel-basis, the CT data is segmented into four material types by using Hounsfield unit (HU) intervals according to table 2. A modification of the HU-based segmentation from DeMarco *et al* (1998) was used. After the HU-based segmentation, voxels in transition regions between air and soft tissue falsely categorized as lung tissue are reassigned by a nearest

neighbor search. Voxels without a neighboring lung voxel within a default distance of three voxels are reassigned to air or soft tissue by a predefined HU value. In cases where a lung volume is contoured on the CT data, all other voxels are reassigned to air or soft tissue. If no pre-segmented lung contour is given, an auto-segmentation is applied by searching for the largest coherent voxel accumulation of lung tissue from the segmentation. Here, using a pre-defined lung contour is favorable.

Material densities are calculated on a voxel basis from HU with a MATLAB function provided by Treeby and Cox (2010) according to Schneider *et al* (1996). A skin layer with default thickness of 1 mm is fitted around the patient by extending the body contour within the patient by a nearest-neighbor-approach. The voxels in this layer are assigned to skin tissue and regardless of the default skin thickness, the minimum layer thickness is one voxel. For the definition of the transport medium, the densities of the four tissue types are set to the mean densities of the voxels assigned to the respective tissue types.

For *BNCT*, a PTV contour named *PTV_BNCT* is required and all associated voxels are automatically re-defined to contain soft tissue with a homogeneous default B-10 concentration of 20 μg per gram tissue. No B-10 is added to voxels outside this contour. The HU intervals for tissue segmentation, the B-10 concentration, and additional simulation parameters are accessible via the MATLAB script *matRad_genVarCT2tissueConversion.m* located in the MCNP folder in matRad. Using this script, the list of tissue types with corresponding HU intervals can be modified by the user to add more tissue types.

2.3. Simulation volume, dose tallies, and transport physics

For the MC simulation, the voxelized simulation volume is set up using MCNP material universes. The simulation voxel dimensions can differ from the voxel dimensions of the CT and can be defined in the matRad graphical user interface (GUI) before the dose calculation. Surrounding the voxel geometry, an air layer of thickness $d_{layer} = 180$ cm is added for source positioning. Particles leaving the simulation volume are deleted so that no back-scattering is considered. The total dose deposition from secondary charged particle interactions within the voxels is recorded using a *TMESH type3* mesh tally. TMESH tallies allow an adequate recording of net energy deposition within each voxel considering all transported primary and secondary particle species entering and leaving or being generated in the voxel. For MCNP accuracy and precision inspection, the *mean, median, and maximum relative errors* for every contoured region of interest in the CT data set are read from the MCNP output and calculated from all voxels with non-zero dose values associated to the respective contours. In

general, relative errors below 10% or even 5% are recommended X-5 Monte Carlo Team (2003) [p. 2-116] for MCNP tallies.

For accurate dose calculations, particle transport is switched on in MCNP using the *MODE-card* for neutrons, photons, electrons, protons, deuterons, ^{3}He, α-particles, and all heavier ions. The default physics settings in MCNP set by the *PHYS-cards* are partly changed for neutrons, photons, and ions. For neutrons, the default *PHYS*-keyword is changed to switch on light-ion recoil and to enable the neutron capture ion algorithm especially important for BNCT (Streitmatter *et al* 2020). Photon physics is changed from default to switch on implicit photonuclear particle production. For protons, light-ion recoil and δ-ray production are activated and for all ions heavier than protons, δ-ray production is also turned on. As recommended in the MCNP manual, the LCA card is used to select CEM03.03 and LAQGSM03.03 models instead of the default model.

In order to use the latest cross section tables provided in the standard package of MCNP version 6.2, the tabulated interaction probabilities and cross sections are loaded from the evaluated nuclear data files (ENDF) database version ENDF/B-VII.1 (Chadwick *et al* 2011) by default. Again, the MATLAB script *matRad_genVarCT2tissueConversion.m* can be modified by the user to change the cross section library for example to the latest ENDF version in case it is available on the user's machine.

The cutoff energies for neutrons, gammas, electrons, protons, and ions are set to $E_{cut,n} = 0.01$ meV, $E_{cut,\gamma} = 3$ keV, $E_{cut,e} = 50$ keV, $E_{cut,p} = 1$ MeV, and $E_{cut,ions} = 1$ MeV, respectively, using the *CUT-card*. Cutoff energies were selected so that the associated mean free path lengths for neutrons and gammas and the ranges obtained with the continuous slowing down approximations for charged particles are well below 1 mm. Therefore, minimum voxel extensions down to 1 mm do not introduce systematic errors.

For variance reduction, the *cell importance* function of MCNP is implemented and the user is provided with the option to change the default cell importance of $IMP = 5$ to tissue-specific values.

2.4. Neutron sources

2.4.1. matRad treatment machines

For the source definition, two options are implemented. As first option, the user can integrate area sources to define radiation fields with particle energy and velocity vector distributions stored in MCNP *RSSA* files from preceding MCNP simulations. While this option - hereinafter referred to as *predefined field approach* - provides the potential to incorporate individual radiation source characteristics, it also needs substantial hands-on activity to account for the particularities of the considered radiation source.

The second option adopts the approach for intensity modulated radiation therapy (IMRT) implemented in matRad for irradiations with an isocentric setup. In this approach - hereinafter referred to as *bixel approach*, the radiation field is subdivided into several quadratic rays of predefined size (bixels). Here, an area source is defined for starting particles in MCNP. The initial energy spectrum is read from the matRad machine file. In the machine file, the user can optionally define a maximum angle for the velocity vector distribution with respect to the surface source normal. In cases where no opening angle is defined, a mono-directional surface source is set in MCNP. The set-up of a pure photon source or a mixed neutron-gamma source is realized in the same way and can be selected with the machine files in matRad.

For BNCT calculations, the user can also define a circular source parameter in the matRad machine file so that the bixel size is interpreted as diameter for the set-up of the surface source. Machine files can also be added in order to include customized neutron spectra.

2.4.2. Neutron sources for demonstration purposes

For demonstration purposes, MC dose calculations were performed for two neutron sources.

FNT treatment at MEDAPP: First, the predefined field approach is used for a retrospective dose calculation for an actual FNT treatment performed in 2012 with fast fission neutrons at the MEDAPP facility in Garching (Wagner *et al* 2008). At MEDAPP, neutrons with a mean energy of $E_n = 1.9$ MeV are generated by fission of uranium ^{235}U so that a mixed neutron-gamma radiation field is applied to the patient. For this example, the treatment field according to the settings of the multi leaf collimator (MLC) was calculated beforehand and recorded at the MLC exit in an RSSA file. The neutron and gamma fluence at irradiation position as investigated by Breitkreutz *et al* (2008) and Jungwirth *et al* (2012) were used as input. In order to simulate the neutron and the gamma dose individually, two separate MC dose calculations were run by reading the respective source particles from the RSSA file. The patient suffered from an adenocystic carcinoma in the submandibular gland and due to the beginning infiltration of the surrounding tissue a large planning target volume (PTV) was contoured on the planning CT. The voxel size of the planning CT scan is 1.5 mm and 3 mm in lateral and axial direction, respectively. For the FNT treatment at MEDAPP with a prescribed combined neutron and gamma dose of 6 Gy delivered in four fractions an irradiation time of 105 sec for each fraction was used in 2012.

BNCT treatment: As a second example, this time for a BNCT scenario, an epithermal neutron spectrum from a D-T neutron generator in combination with an ideal beam shaping assembly as discussed by Verbeke *et al* (2000) was used. The source was defined as one monodirectional circular field with a diameter of 45 mm. The same planning CT from the retrospective example was used.

In the contour set, the submandibular gland was renamed to *PTV_BNCT* so that it is recognized by the dose engine as PTV for BNCT and the PTV was deleted. The ^{10}B-concentration was increased from the default value to 30 μg per gram tissue and the cross section library was changed to ENDF/B-VIII.0 including the fix for the ^{10}B cross section (LANL 2022). The dose deposition was optimized to a mean physical dose of 6 Gy in the new BNCT PTV.

3. Results

3.1. Dose calculation example for fast neutron therapy at MEDAPP

Segmentation and post-processing results

The planning CT for the retrospective dose calculation contains Hounsfield Units ranging from $HU_{\min} = -1000$ to $HU_{\max} = 3071$. After the automatic segmentation based on HU intervals, a skin layer with the default thickness was added. The data set contains a total number of 607569 voxels. The calculated mean densities for the three tissue types soft tissue (st), skin (sk), and bone (b) are $\rho_{st,mean} = (1.007 \pm 0.115)$ g cm^{-3}, $\rho_{sk,mean} = (1.014 \pm 0.260)$ g cm^{-3}, and $\rho_{b,mean} = (1.555 \pm 0.348)$ g cm^{-3}.

The *contour information* including the automatic segmentation into the three main tissue types is given as overlay on the CT data in figure 2. For the MC calculation, all voxels inside the patient except for air cavities, the contoured bone, and skin regions are passed to MCNP as soft tissue. This means the elemental composition of other manually contoured regions like the PTV and the myelon shown in figure 2 is identical to soft tissue. The matRad isocenter is indicated by the black cross.

Retrospective dose calculation

According to the records of the irradiation position of the patient, the surface source was positioned using the pre-calculated RSSA file at a distance of 54 cm from the patient surface. The calculated total neutron and gamma dose for one fraction is shown in axial view in figure 3. Here, isodose lines indicate doses from 0.25 Gy to 1.25 Gy with equal spacing of 0.25 Gy. The maximum total dose was calculated to be $D_{\max} = 1.499$ Gy which nearly coincides with the prescribed dose per fraction of $D = 1.5$ Gy. A maximum neutron dose of $D_{n,\max} = 1.269$ Gy and a maximum gamma dose of $D_{\gamma,\max} = 0.321$ Gy are reported.

For a quantitative evaluation, the DVH was calculated with matRad and is shown in figure 4. For example, 95% of the PTV volume are covered by 0.735 Gy and 50% by 1.227 Gy. The maximum dose to organs at risk like the brainstem, larynx, myelon, and skin
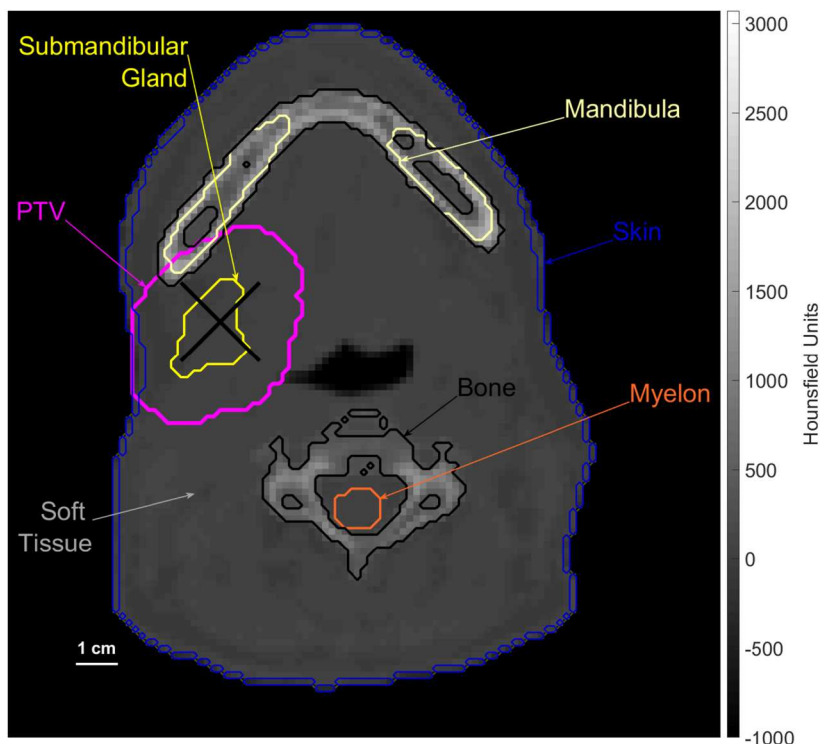
Figure 2. Axial view of the planning CT for retrospective dose calculation including manually contoured regions of interest and tissue types from auto-segmentation. The isocenter is indicated as black cross.
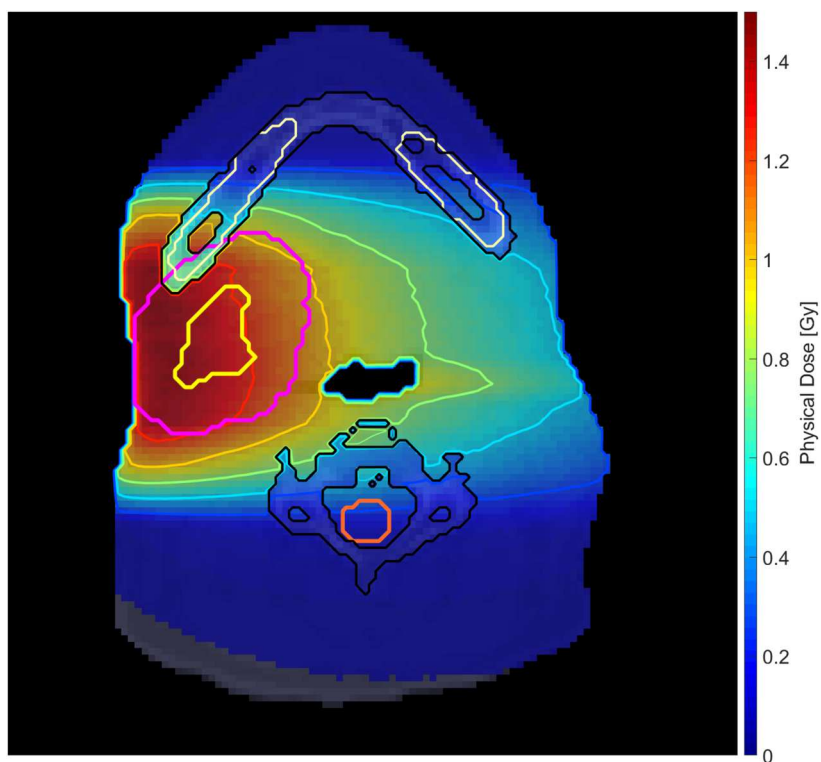

Figure 3. Result of retrospective total dose calculation using MCNP for one fraction.

were calculated to be 0.070 Gy, 0.988 Gy, 0.411 Gy, and 1.418 Gy, respectively. The mean dose to the larynx is 0.463 Gy.

Computational aspects of retrospective dose calculation
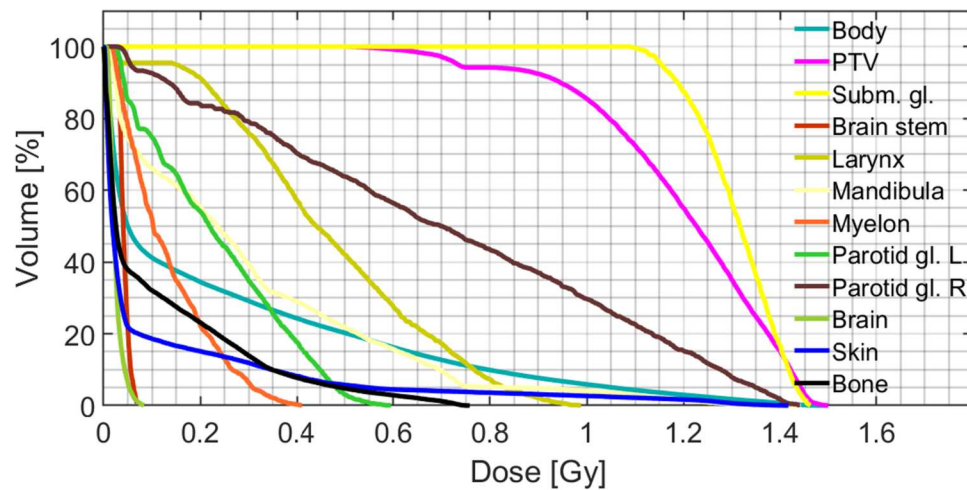The MC calculations and data storage operations for the individual beam components were executed by

Figure 4. DVH calculated from retrospective dose calculation using MCNP.

Table 3. Maximum, mean, and median relative error information calculated from MCNP tally-output for the two beam components for selected contours.

	Neutron statistics (rel. error)			Gamma statistics (rel. error)		
	maximum	mean	median	maximum	mean	median
Body	100%	2.2%	1.4%	100%	5.6%	3.8%
PTV	1.8%	0.7%	0.7%	5.5%	0.8%	0.7%
Subm. gland	0.8%	0.7%	0.7%	0.8%	0.7%	0.7%
Brainstem	5.3%	1.1%	1.1%	13.3%	4.3%	4.4%
Laryxn	98.3%	2.8%	1.2%	100%	2.7%	1.1%
Mandibula	2.9%	1.2%	1.1%	19.1%	1.8%	1.0%
Myelon	2.4%	1.1%	1.1%	27.2%	2.8%	2.4%
Brain	15.4%	1.6%	1.5%	60.9%	5.9%	5.8%
Bone	36.6%	3.0%	1.5%	80.0%	4.9%	3.6%

MCNP for neutrons and gammas within a time of $8 - 12$ h for 1.1×10^7 starting particles read from the RSSA file. The calculation was executed in parallel mode using 20 CPUs of the virtual machine. About 20 GB of RAM were sufficient to run the individual simulations. In general, the RAM requirements will depend on the size of the computational grid and the size of the RSSA file.

For both beam components, relative error information is provided in table 3. *Maximum, mean, and median relative errors* are given for the whole body - i.e. all voxels inside the body contour - and for selected volumes of interest like the PTV or the brainstem. As indicated in table 3, the 5%-criterion is met for the mean relative error for all contours except the brain.

3.2. Dose calculation example for boron neutron capture therapy

BNCT dose calculation
For the BNCT example, the calculated total dose is shown in axial view in figure 5 where the original PTV is deleted and the new PTV for BNCT coincides with the submandibular gland contour. With the optimization to a mean dose of $D_{mean} = 6.0$ Gy in the new

PTV, a maximum physical dose of $D_{max} = 6.9$ Gy was calculated. Isodose lines are plotted between 0.5 Gy and 6.5 Gy with spacing of 0.5 Gy.

The DVH as computed with matRad is shown in figure 6. For the hypothetical scenario shown here where B-10 is only enriched in the PTV, significant sparing of the organs at risk surrounding the PTV is observed. High maximum dose values above 2 Gy were calculated for the skin, the mandibula, the right parotid gland, and bone. Since no overlap with the PTV for BNCT exists and therefore no B-10 is present in these contours, the dose deposition in these organs in due to irradiation with neutrons.

Computational aspects of BNCT dose calculation
The dose calculation and tally processing for 2×10^8 starting neutrons took around 16 hours using 42 CPUs. The relative error information for the dose calculation is provided in table 4. *Maximum, mean, and median relative errors* are given for the body contour and for selected contours like the new PTV for BNCT. The 5%-criterion is met for the mean relative error for all contours except the brain.
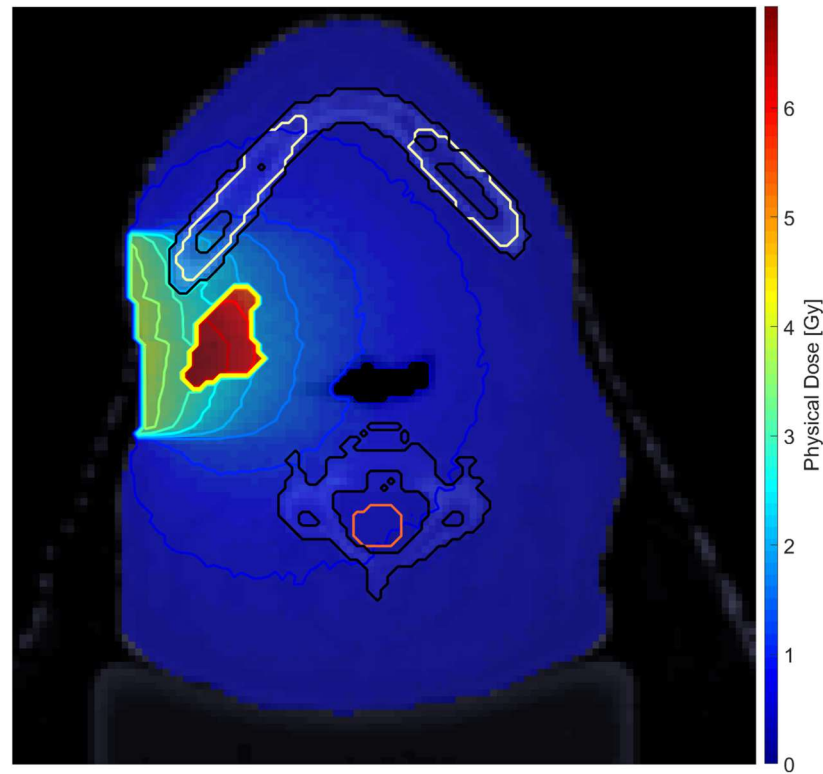
Figure 5. Result of total dose calculation using MCNP for a BNCT field. The submandibular gland is redefined with a B-10 concentration of 30 μg g^{-1}. The optimization was performed with the objective of a mean PTV dose of 6 Gy.

4. Discussion

4.1. CT processing and segmentation

Within the standard deviation, the calculated mean densities $\rho_{st,mean} = (1.007 \pm 0.115)$ g cm^{-3}, $\rho_{sk,mean} = (1.014 \pm 0.260)$ g cm^{-3}, and $\rho_{b,mean} = (1.555 \pm 0.348)$ g cm^{-3} agree with the reference values $\rho_{st,NIST} = 1.000$ g cm^{-3}, $\rho_{sk,NIST} = 1.100$ g cm^{-3}, and $\rho_{b,NIST} = 1.850$ g cm^{-3} provided by NIST NIST (2022). Here, the difference between the mean density calculated for soft tissue and the reference value is below 1% and therefore negligible. For skin and bone, calculated densities are about 8% respectively 16% lower than the reference values.

Given the large standard deviations especially for bone and skin tissue, further advancement of the conversion of HU to density and the whole segmentation process is advisable. This could be realized by adopting the method suggested by Schneider *et al* (2000). For the segmentation, the HU scale is there divided into 24 bins and used as input for Monte Carlo simulations. Also, Schneider *et al* (2000) used densities calculated for each voxel individually.

4.2. Retrospective dose calculation

As expected, good agreement with the prescribed maximum dose in the PTV for one fraction was achieved with the predefined field approach for the retrospective dose calculation. As shown in figure 3, the dose deposition from the mixed neutron gamma

radiation field in bone tissue is significantly reduced. This is due to the low hydrogen content in bone in comparison to soft tissue.

With the performance evaluation of the Monte Carlo dose calculation approach in water in a preceding work (Sommer *et al* 2024) using the same geometry of the MEDAPP beam tube, good confidence exists in the predefined field approach. This holds true even though the designs of the MLC used in Sommer *et al* (2024) and the one used for the retrospective calculation differ. Nevertheless, a verification in heterogeneous media is pending. Unfortunately, this was not possible due to an ongoing shutdown of FRM II since 2020.

For retrospective evaluation of FNT treatments with fast fission neutrons at MEDAPP, the presented dose calculation approach can be used for the inspection of the dose distribution including the evaluation using DVHs. Running two simulations for the respective beam components offers the benefit to separate between dose deposition from primary neutron and gamma radiation. While only available for retrospective evaluation, the results from the dose calculation will be valuable to correlate the outcome of the follow up with the reported dose.

4.3. BNCT dose calculation

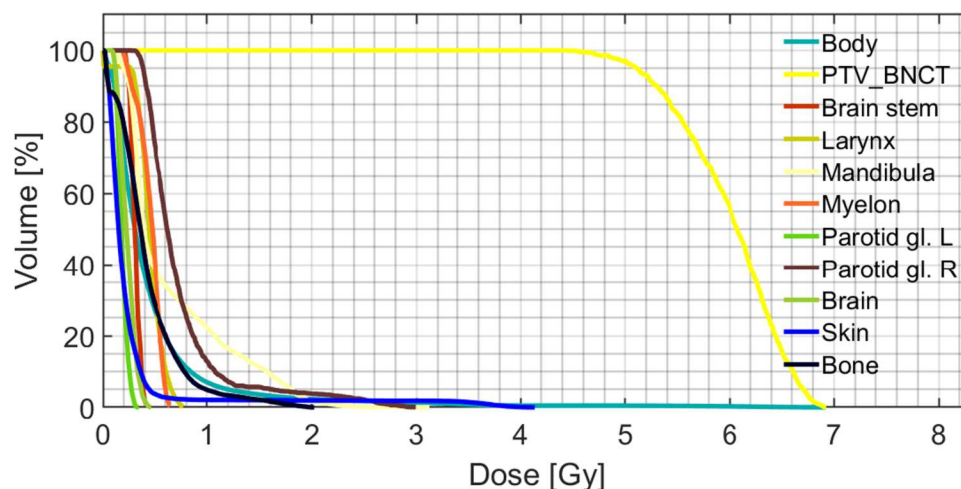As reported in figure 5 and the DVH in figure 6, the general benefits of BNCT regarding selective dose

Figure 6. DVH calculated from BNCT dose calculation using MCNP.

Table 4. Maximum, mean, and median relative error information calculated from MCNP tally-output for selected contours.

	Neutron statistics (rel. error)		
	maximum	mean	median
Body	100%	4.8%	4.1%
PTV/Subm. gland	0.5%	0.4%	0.4%
Brainstem	5.3%	4.3%	4.3%
Laryxn	100%	3.7%	3.4%
Mandibula	7.3%	3.1%	3.3%
Myelon	5.5%	3.5%	3.3%
Brain	10.4%	5.2%	5.0%

deposition is shown. Nevertheless, the restriction of B-10 into the tumor volume is an oversimplification.

Here, the BNCT example only gives an impression of the dose calculation options now introduced for BNCT with matRad and the chosen bixel approach using a mono-directional neutron beam is not a realistic scenario. It should be noted that at this point only the total dose from MCNP is available within matRad while for an accurate BNCT dose calculation, the separation of the dose into contributions from B-10 neutron capture, secondary gammas, fast neutrons, and thermal neutron capture reactions by nitrogen is crucial (IAEA 2023).

4.4. Relative computational errors

Since the simulation volume is separated into a large number of voxels that are partly located outside the irradiation site, the criterion for relative errors below 10% cannot be matched for all voxels in a reasonable computation time. Nevertheless, maximum, mean, and median values as reported in matRad given in tables 3 and 4 allow an insight into the precision and partly also into the accuracy of the dose calculations.

For some volumes of interest like the larynx and for the whole body maximum relative errors up to 100% are reported. The main reason for that are unavoidable large uncertainties in voxels outside the irradiation field.

To gain confidence about the simulation outcome in terms of the relative error, it should be sufficient to run simulations with a large enough number of starting particles to achieve mean and median errors of around 10% as recommended for MCNP. For both examples the number of starting particles was set high enough to reach relative errors around 5%. For the retrospective FNT example 1.1×10^7 starting particles were set and for the BNCT example 2×10^8.

In all cases the maximum error should be examined carefully with regard to the location of the considered volume. In case a large maximum error is reported for a structure located directly within the irradiation field, the simulation input should be revisited. In such cases, the sampling of regions of interest inside the radiation field is likely to be inaccurate.

In addition to the MC statistics, the accuracy of the dose calculation is influenced by the input spectrum, the velocity vector distribution written to the RSSA file, and the approximations made with the bixel approach.

4.5. Customization and potential for research

The open source approach of matRad and the already introduced options for customization of the machine file give a good starting point for the use in BNCT research with a homogeneous B-10 concentration in the PTV. To allow dose calculation with heterogeneous B-10 concentrations, a user could modify the list of predefined materials and the segmentation function to recognize additional contours with predefined B-10 concentrations and specific names.

Treatment planning for research purposes with matRad is easy to use and the neutron spectra included in the machine files are easy to adopt without required knowledge of MCNP. For advanced users,

the option to include predefined source files provides high flexibility for customization.

matRad also supports dose calculation for different radiation modalities including photons and charged particles. Results from treatment planning can be saved from the GUI to the matRad-specific MATLAB variables. The dose calculation results including RBE weighted dose where available for different radiation modalities can then be inspected directly in the GUI or processed further in MATLAB. To generate multi-modal treatment plans, summation of the matRad-specific MATLAB variables containing results for different modalities is possible with basic MATLAB knowledge and results can be inspected in the matRad GUI.

5. Conclusion

With the presented MC neutron dose engine for matRad, a general purpose implementation for dose calculation for FNT and BNCT is introduced based on the well established particle transport code MCNP. Here, the *DoseEngine* infrastructure of matRad allowed the addition of the new neutron modality.

The discussed technical requirements to run dose calculations with acceptable MC statistics in a reasonable runtime of less then 24 h for one field should pose no significant obstacle in terms of hardware costs.

The dose calculation is limited to the total physical dose. In order to allow the separation of different dose components important for neutron therapy, the advancements of the MC dose engine to include particle specific tallies for individual inspection and RBE modeling is pursued.

In addition, the verification of the dose calculation approach in heterogeneous media is planned for the future.

Acknowledgments

Data availability statement

All data that support the findings of this study are included within the article (and any supplementary files).

References

Abbani N *et al* (2024) *matRad (v3.1.0)* Zenodo:10.5281/zenodo.14181851

Aljabab S, Lui A, Wong T, Liao J, Laramore G and Parvathaneni U 2021 *Cureus* **13** e14844

Anderson A *et al* 2023 *Int. J. Radiat. Oncol. Biol. Phys.* **117** e561–2

Barth R F, Wu G, Maria da Graca H V, Grecula J C and Gupta N 2024 *Cancer Communications* **44** 889

Breitkreutz H, Wagner F M, Röhrmoser A and Petry W 2008 *Nucl. Instrum. Methods Phys. Res.* A **593** 466–71

Chadwick M B *et al* 2011 *Nucl. Data Sheets* **112** 2887–996

DeMarco J, Solberg T and Smathers J B 1998 *Med. Phys.* **25** 1–11

Gordon K, Gulidov I, Fatkhudinov T, Koryakin S and Kaprin A 2022 *International Journal of Particle Therapy* **9** 59–69

Gulidov I, Koryakin S, Fatkhudinov T and Gordon K 2023 *Int. J. Radiat. Oncol. Biol. Phys.* **115** 821–7

Han Y, Geng C, Altieri S, Bortolussi S, Liu Y, Wahl N and Tang X 2023 *Phys. Med. Biol.* **69** 015024

IAEA 2023 *Advances in Boron Neutron Capture Therapy* (Non-serial Publications International Atomic Energy Agency) https://www.iaea.org/publications/15339/advances-in-boron-neutron-capture-therapy

ICRU 1992 *Report 46: Photon, Electron, Proton and Neutron Interaction Data for Body Tissues* Journal of the International Commission on Radiation Units and Measurements os24

Jones B 2020 *Frontiers in Oncology* **10** 1537

Jones D and Wambersie A 2007 *Nucl. Instrum. Methods Phys. Res.* A **580** 522–5

Jungwirth M, Breitkreutz H, Wagner F M and Bücherl T 2012 *J. Instrum.* **7** C03022–03022

Kalet A M, Sandison G A, Phillips M H and Parvathaneni U 2013 *Journal of Applied Clinical Medical Physics* **14** 133–54

LANL 2022 https://nucleardata.lanl.gov/ace/lib80x/ [2024-11-18]Lib80x—Library based on ENDF/B-VIII.0

Lehnert A L, Kranz M E, DeWitt D Q, Argento D C, Stewart R D and Miyaoka R S 2025 An Imaging System to Support Fast Neutron Therapy Quality Assurance (QA) of Intensity Modulated Neutron Therapy (IMNT) *IEEE Trans. Radiat. Plasma Med Sci.* **9** 970–7

Loap P and Kirova Y 2021 *International Journal of Particle Therapy* **7** 61–4

Locher G L 1936 *The American Journal of Roentgenology and Radium Therapy* **36** 1–13

Moffitt G B, Sandison G A, Argento D C, Emery R, Wootton L S, Parvathaneni U, Liao J J, Laramore G E and Stewart R D 2023 *Phys. Med. Biol.* **68** 245011

Moffitt G B, Stewart R D, Sandison G A, Goorley J T, Argento D C, Jevremovic T, Emery R, Wootton L S, Parvathaneni U and Laramore G E 2018 *Phys. Med. Biol.* **63** 105008

Moffitt G B, Wootton L S, Hårdemark B, Sandison G A, Laramore G E, Parvathaneni U and Stewart R D 2020 *Phys. Med. Biol.* **65** 165009

Neuboron 2024 https://en.neuboron.com/bnct [2024-11-25]TPS advertised at webpage

NIST 2022 https://physics.nist.gov/cgi-bin/Star/compos.pl?matno=001 [2022-01-11]National institute of standards and technology: material composition data

RaySearch 2024 https://raysearchlabs.com/boron-neutron-capture-therapy/ [2024-11-25]TPS advertised at webpage

Sandison G *et al* 2023 *Int. J. Radiat. Oncol. Biol. Phys.* **117** e714

Sauerwein W A, Fischer T, Sancey L, Verry C, Matsuura E, Moss R L and Wittig A 2023 *Bio-Algorithms and Med-Systems* **19** 48–53

Schneider U, Pedroni E and Lomax A 1996 *Phys. Med. Biol.* **41** 111

Schneider W, Bortfeld T and Schlegel W 2000 *Phys. Med. Biol.* **45** 459

Sommer L B, Kampfer S, Chemnitz T, Breitkreutz H, Combs S E and Wilkens J J 2024 *Phys. Med. Biol.* **69** 045022

Specht H M, Neff T, Reuschel W, Wagner F M, Kampfer S, Wilkens J J, Petry W and Combs S E 2015 *Frontiers in Oncology* **5** 262

Stewart R D, Carlson D J, Butkus M P, Hawkins R, Friedrich T and Scholz M 2018 *Med. Phys.* **45** e925–52

Streitmatter S W, Stewart R D, Moffitt G and Jevremovic T 2020 *Cells* **9** 2302

Suzuki M 2020 *International Journal of Clinical Oncology* **25** 43–50

Treeby B E and Cox B T 2010 *J. Biomed. Opt.* **15** 021314

Verbeke J, Vujic J and Leung K 2000 *Nucl. Technol.* **129** 257–78

Wagner F M, Kneschaurek P, Kastenmüller A, Loeper-Kabasakal B, Kampfer S, Breitkreutz H, Waschkowski W, Molls M and Petry W 2008 *Strahlentherapie und Onkologie* **184** 643–6

Werner C J 2017 *Los Alamos National Laboratory, Los Alamos, NM, LA-UR-17-29981*

Wieser H P *et al* 2017 *Med. Phys.* **44** 2556–68

X-5 Monte Carlo Team 2003 *Los Alamos National Laboratory, Los Alamos, NM, LA-UR-03-1987*